small
NANO MICRO

Tumor-Responsive Fluorescent Light-up Probe Based on a Gold Nanoparticle/Conjugated Polyelectrolyte Hybrid

*Youyong Yuan, Dan Ding, Kai Li, Jie Liu, and Bin Liu**

***A** tumor-responsive nanoprobe based on a conjugated polyelectrolyte and gold nanoparticle (AuNP) hybrid was designed to response to the low pH extracellular microenvironment in tumor with light-up fluorescence. AuNPs with positive surface charges were prepared by direct reducing Au salt with sodium borohydride and stabilized by cystamine. A pH triggered charge-reversible polymer and a water-soluble cationic conjugated polyelectrolyte (CPE) were sequentially deposited onto the AuNP surface through electrostatic interaction. The obtained hybrid probe is monodispersed with an average diameter of 68.3 nm by dynamic light scattering measurement. In physiological conditions (pH ≈ 7.4), the hybrid probe is almost non-fluorescent due to the super-quenching of CPE by AuNPs via energy/charge transfer and efficient exciton migration along the polymer backbone. When exposed to acidic extracellular microenvironments in tumor (pH_e ≈ 6.5), the acid-labile amides hydrolyze into primary amines. The generated amine groups result in strong electrostatic repulsion between CPE and AuNPs, leading to recovered probe fluorescence. The fluorescence turn-on is further utilized for tumor extracellular acidic microenvironment imaging. In addition, under in vivo conditions, the nanosized hybrid probe exhibits specific accumulation in tumor tissue with light-up fluorescence, which provides new opportunities for easy tumor imaging and identification.*

1. Introduction

Stimulus-responsive probes have been developed for specific tumor imaging.[1,2] To achieve high signal-to-background ratio, most of them are designed to be fluorescently quenched at a quiescent stage but activated when encountering a specific trigger, which leads to structural or conformational changes to restore the fluorescence. The specific triggers are usually enzymes[3–6] or pH.[7–11] In particular, tumor-related enzyme activatable probes have been widely used in tumor imaging.[3–6] However, as most tumor-related enzymes are also presented in normal physiological tissues, these probes often yield undesirable background signals. Recently, non-invasive imaging of low pH microenvironment has attracted much attention as a new means of early diagnosis of diseases, evaluation of disease progression and therapy efficiency.[10,11] Among them, the tumor extracellular microenvironment is more acidic (pH_e ≈ 6.5) than normal tissue (pH ≈ 7.4), which is an important character of various tumors.[12] To visualize the pH microenvironment of tumors,[13] various molecular probes have been developed for magnetic resonance imaging (MRI),[14–16] positron emission tomography (PET),[17] and optical imaging.[11] However, most of them are targeted for the intracellular pH (pH ≈ 5.5), instead of the tumor extracellular pH. It remains challenge to design a probe targeting tumor extracellular acidic microenviroment, because of the

Dr. Y. Yuan, Dr. D. Ding, Dr. J. Liu and Prof. B. Liu
Department of Chemical and
Biomolecular Engineering
National University of Singapore
4 Engineering Drive 4, Singapore 117576
Tel: (+65) 6516–8049, Fax: (+65) 6779–1936
E-mail: cheliub@nus.edu.sg
Dr. K. Li and Prof. B. Liu
Institute of Materials Research and Engineering
3 Research Link, Singapore 117602

DOI: 10.1002/smll.201302765

small pH difference between the tumor extracellular tissue and normal ones.

Conjugated polyelectrolytes (CPEs) are macromolecules with π-delocalized backbones and ionic side chains, which provide a novel platform for a variety of biological sensing and imaging applications.[18–22] CPEs inherit the intrinsic properties of conjugated polymers with tunable absorption and emission spectra, which exhibit molecular wire effect due to rapid exciton transport along the conjugated backbones.[23] This allows the CPE fluorescence to be effectively quenched in the presence of quenchers, such as small organic molecules or gold nanoparticles (Au NPs). In addition, the ionic pendent groups of CPE render the polymers highly soluble or dispersible in aqueous media, which is essential for chemical and biological sensing.[24–26] These unique features have inspired us to design stimulus-responsive light-up probes based on CPE and Au NPs for tumor imaging.

In this contribution, we report the rational design of a pH-responsive Au NP and CPE hybrid probe for tumor acidic extracellullar microenvironment imaging. The Au NPs with positive surface charges were prepared in one pot and sequentially coated with a pH-responsive charge-reversible polymer and a cationic CPE through electrostatic interaction. The hybrid probe is almost non-fluorescent in physiological conditions (pH ≈ 7.4) due to the super-quenching of CPE by AuNPs. When exposed to acidic microenvironment in tumor (pH ≈ 6.5), the acid-labile amides hydrolyze into primary amines. The generated amine groups result in strong electrostatic repulsion between CPE and AuNPs, leading to fluorescence turn-on. Both in vitro and in vivo studies showed that our probe can be utilized for tumor extracellular acidic microenvironment imaging.

2. Results and Discussion

To synthesize the pH-responsive (or charge-reversible) polymer, firstly, we obtained poly(L-lysine)-*graft*-poly(ethylene glycol) (PLL-*g*-PEG) copolymer by conjugating *N*-hydroxysuccinimide (NHS) activated PEG to ε-amine groups in poly-(L-lysine) (PLL).[27] The grafting percentage of PEG to the PLL side chain was about 8%, as calculated from the ^{1}H NMR spectrum. The charge-reversal polymer (PLL-*g*-PEG/DMA) was synthesized by conjugating the residual primary amine groups of PLL with 2,3-dimethylmaleic anhydride (DMA) to form acid-labile amides,[28,29] which was purified by precipitation in a mixed solvent of diethyl ether and acetone. The structure of PLL-*g*-PEG/DMA was characterized by ^{1}H NMR spectroscopy and the degree of amidization was higher than 95%. Using a similar strategy, by replacing 2,3-dimethylmaleic anhydride with succinic anhydride (SA), PLL-*g*-PEG/SA was also obtained as a control polymer.

Gold nanoparticles has been widely used for biomedical applications.[30–33] In this work, cysteamine-capped AuNPs were prepared by reducing chloroauric acid ($HAuCl_4$) with sodium borohydride ($NaBH_4$) in the presence of cysteamine as stabilizer.[34] The as-prepared AuNPs are wine-red in color and show a maximum absorption peak at 526 nm (**Figure 1**A), which is ascribed to the surface plasmon resonance of the AuNPs. Transmission electron microscopy

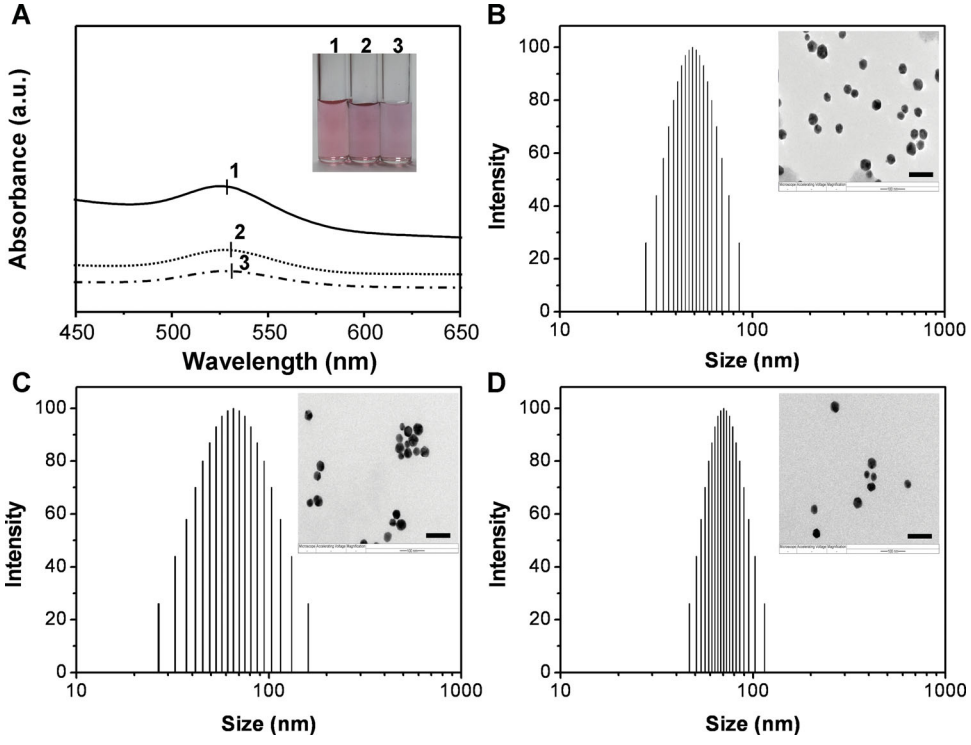

Figure 1. (A) UV-vis spectra of the Au NPs (1), PFBT/PLL-*g*-PEG/DMA/AuNPs (2) and PFBT/PLL-*g*-PEG/SA/AuNPs (3). Inset shows the photos of the corresponding solution. Representative hydrodynamic diameters of the AuNPs (B), PFBT/PLL-*g*-PEG/DMA/AuNPs (C) and PFBT/PLL-*g*-PEG/SA/AuNPs (D) measured by laser light scattering. Insets show the corresponding TEM iamges (scale bar = 100 nm).

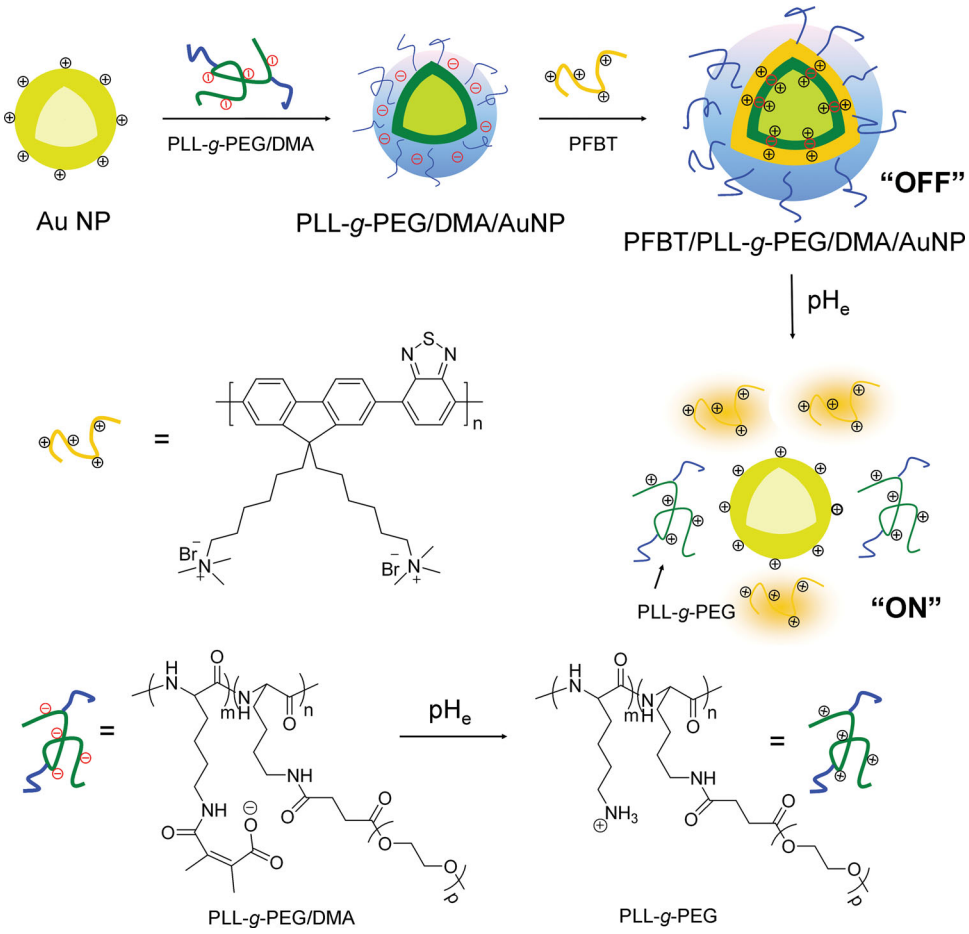

Scheme 1. Schematic illustration of the PFBT/PLL-*g*-PEG/DMA/AuNP fabrication and its tumor-acidity-activated fluorescence light-up. pH_e: tumor extracellular pH.

(TEM) and dynamic light scattering (DLS) measurements show that the Au NPs are spherical in shape with sizes of 49 nm in diameter (Figure 1B). In addition, the zeta potential of the Au NPs is positive (+43.7 mV) due to the presence of positively charged $–NH_3^+$ groups on NP surface.

The pH-responsive Au NP hybrid was prepared by firstly adsorption of anionic polyelectrolyte PLL-*g*-PEG/DMA to the positively charged AuNPs, which was followed by the self-assembly of a cationic CPE of poly[9,9-bis(6′-*N*,*N*,*N*-trimethylammonium)hexyl)fluorene-*alt*-4,7-(2,1,3-benzothiadiazole) dibromide] (PFBT) (**Scheme 1**). PFBT was selected because it is positively charged and water soluble, which has an absorption maximum at 440 nm, matching the 457 nm laser equipped on the confocal microscopy. In addition, it shows a large Stokes shift of 117 nm, which is ideal for fluorescence imaging. The process of polyelectrolyte deposition on AuNPs in each step was monitored by UV-vis spectra, DLS and TEM (Figure 1). The very minor plasmon absorbance change in the AuNP (from 526 to 529 nm) after polymer deposition indicates low levels of aggregation in the procedure, which is also reflected by the wine-red color for the Au NPs after each step. DLS results show that the nanoparticle size is slightly increased from 49 nm for naked AuNPs to 68.3 nm for the hybrid. The particle size distribution after the coating stays monodispersed with a polydispersity index (PDI) of 0.315. TEM analyses of each step showed similar results. The control probe, PFBT/PLL-*g*-PEG/SA/AuNP, was also synthesized and characterized to be monodispersed (Figure 1D).

To test the pH-responsive cleavage of the amide bond in this study, we incubated the probes in buffers with pH 6.5 and 7.4, and monitored their surface potential changes with time. As shown in **Figure 2**A, the zeta potential of PFBT/PLL-*g*-PEG/DMA/AuNPs upon incubation at pH 6.5 increases quickly from –3.2 mV to 23.3 mV within 60 minutes and the rate constant of zeta potential change calculated to be 0.540 mV min^{-1} based on the linear fit of the initial 40 mins. The same probe incubated at pH 7.4 shows a minimal surface charge change within two hours and the rate constant of zeta potential change is 0.149 mV min^{-1}, which is one third of that at pH 6.5, demonstrating slower hydrolysis of PLL-*g*-PEG/DMA at pH 7.4. In contrast, PFBT/PLL-*g*-PEG/SA/AuNPs do not exhibit charge reversal upon incubation at pH 7.4 or 6.5 (Figure 2B).

It is hypothesized that the charge reversal of the polymer layer could lead to the release of PFBT from the vicinity of the AuNPs to enhance the solution fluorescence. To validate the hypothesis, PFBT/PLL-*g*-PEG/DMA/AuNPs were incubated in PBS at pH 6.5 and 7.4, and the fluorescence intensities (λ_{ex} = 440 nm) were monitored at different time points. PFBT/PLL-*g*-PEG/DMA/AuNPs show very low fluorescence

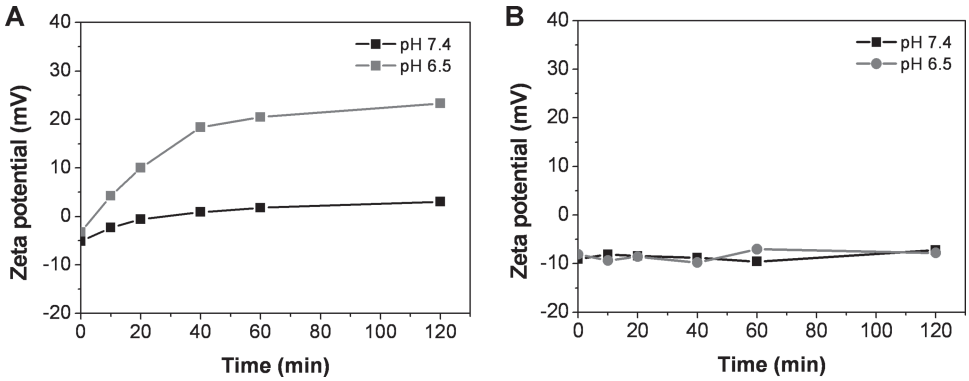

Figure 2. Zeta potential change of PFBT/PLL-*g*-PEG/DMA/AuNPs (A) and PFBT/PLL-*g*-PEG/SA/AuNPs (B) after incubation at pH 7.4 or 6.5 for different time.

at pH = 7.4, due to the super quenching of PFBT by Au NPs.[35] However, when the same probe is incubated at tumoral acidic pH of 6.5, it shows time-dependent fluorescence recovery due to the charge reversal of the PLL-*g*-PEG/DMA from negative to positive, which releases PFBT from the hybrid. As shown in **Figure 3**A, at pH = 6.5, the solution fluorescence increases significantly as a result of the amide bond hydrolysis, reaching a maximum with 8.2-fold enhancement within 1 h. In contrast, PFBT/PLL-*g*-PEG/DMA/AuNPs remain in the quenched state for up to 1.5 h at pH 7.4 (Figure 3B). The rate constant of fluorescence intensity change at pH 6.5 is calculated to be 0.552 a.u. min^{-1}, which is 10.6 times quicker than that at pH 7.4 (0.052 a.u. min^{-1}). The control probe of PFBT/PLL-g-PEG/SA/AuNPs does not show any pH-responsive fluorescence recovery upon incubation at pH 6.5 (Figure 3C) or 7.4 (Figure 3D). These results indicate that the amide bond formed between amine and DMA functional groups is essential for charge-reversal of the hybrid to yield fluorescence.

The PFBT/PLL-*g*-PEG/DMA/AuNPs were subsequently cultured with cells in cell culture medium at pH 7.4 or 6.5 and the fluorescence of the cells was studied by confocal microscopy. As shown in **Figure 4**A, after incubating the PFBT/PLL-*g*-PEG/DMA/AuNPs with U87-MG cells at pH 6.5 for 1 h, strong yellow fluorescence is observed inside the cells. Under the same experimental conditions, no significant fluorescence could be observed at pH 7.4 (Figure 4B). As control, PFBT/PLL-*g*-PEG/SA/AuNPs treated tumor cells do not show any

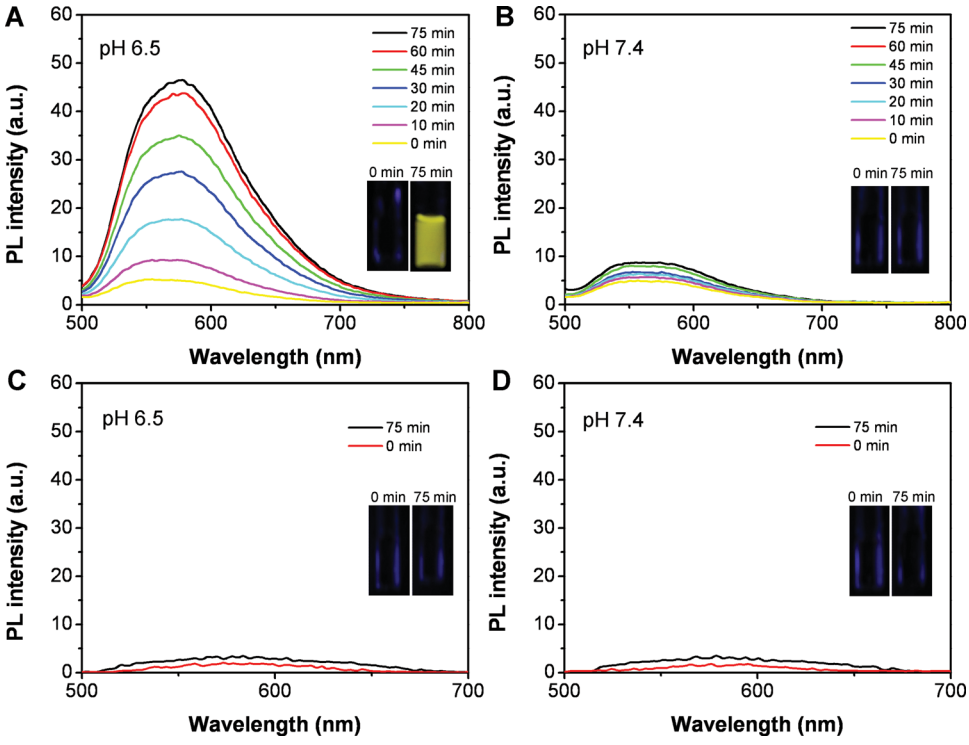

Figure 3. Time-dependent fluorescence spectra of PFBT/PLL-*g*-PEG/DMA/AuNPs at pH 6.5 (A) or pH 7.4 (B); Time-dependent fluorescence spectra of PFBT/PLL-*g*-PEG/SA/AuNPs hybrid at pH 6.5 (C) or pH 7.4 (D). Insets: Photographs of PFBT/PLL-*g*-PEG/DMA/AuNPs or PFBT/PLL-*g*-PEG/SA/AuNPs taken at t = 0 and 75 minutes under illumination of a UV lamp at 365 nm.

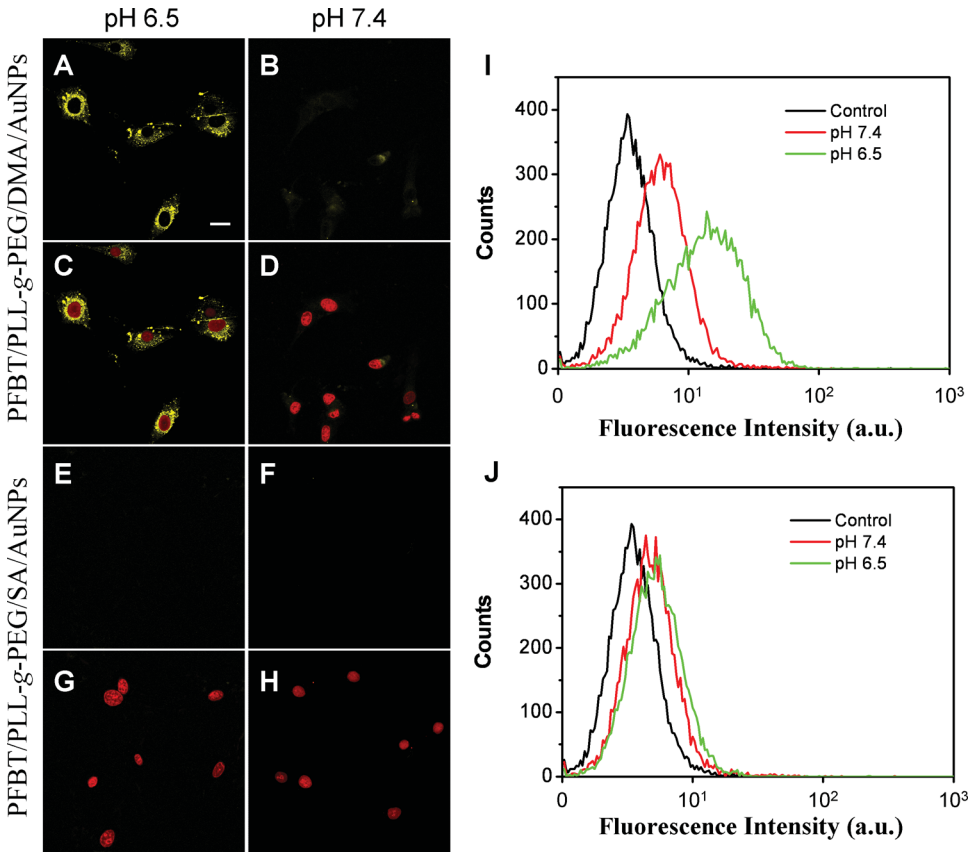

Figure 4. Confocal images of U87-MG cells incubated with PFBT/PLL-*g*-PEG/DMA/AuNPs (A, B) or PFBT/PLL-*g*-PEG/SA/AuNPs (E, F) at pH 6.5 (A, E) or pH 7.4 (B, F) for 1 h. Propidium iodide was used to stain cell nuclei. (C, D) and (G, H) are the corresponding fluorescence/nucleus overlay images of (A, B) and (E, F), respectively. All images share the same scale bar (20 μm). Flow cytometric analyses of U87-MG cells incubated with PFBT/PLL-*g*-PEG/DMA/AuNPs (I) or PFBT/PLL-*g*-PEG/SA/AuNPs (J) at pH 6.5 or pH 7.4 for 1 h. Control samples refer to cells without any treatment.

fluorescence signal at both pH values (Figure 4E– 4H). These results indicate that the AuNP hybrids are responsive to pH in cellular environment.

The enhanced fluorescence intensity of PFBT/PLL-*g*-PEG/DMA/AuNPs upon incubation with U87-MG cells at pH 6.5 was further quantified by flow cytometry. Under the same conditions, the intensity of PFBT fluorescence is 2.8-fold brighter in cells cultured at pH 6.5 as compared to that at pH 7.4 (Figure 4I). In contrast, no difference is observed when the cells are incubated with PFBT/PLL-*g*-PEG/SA/AuNPs at both pH values (Figure 4J). These results are in well accordance with the confocal images.

The in vitro studies demonstrated that PFBT/PLL-*g*-PEG/DMA/AuNPs have good pH- dependent fluorescence light-up to U87-MG cancer cells, which motivated us to further investigate their in vivo performance. It has been reported that nanosized particles can accumulate at the tumor site by enhanced permeability and retention (EPR) effect.[36] Mice bearing C6 glioma tumors were administrated with AuNP hybrid via intravenous administration. After 24 h, the mouse was subsequently imaged by the Maestro imaging system. The mouse autofluorescence was removed by spectral unmixing with the Maestro software. **Figures 5**A shows the in vivo biodistribution profile and tumor accumulation of PFBT/PLL-*g*-PEG/DMA/AuNPs in C6 tumor bearing mice. The tumor accumulation of PFBT/PLL-*g*-PEG/DMA/AuNPs should be due to passive targeting through EPR effect, then the fluorescence of nanoparticles are turn-on in acidic tumor microenvironment. Figure 5B shows the ex vivo fluorescence image of various organs and tissues from C6 tumor-bearing mice intravenously injected with PFBT/PLL-*g*-PEG/DMA/AuNPs at 24 h post-injection. The tissues including kidney, heart, intestine, liver, lung, spleen and tumor were isolated to study the tissue distribution of the NPs. Obvious fluorescent signal is only observed in tumor tissues at 24 h post-injection, while there is almost no detectable fluorescence from other tissues. These results indicate that PFBT/PLL-*g*-PEG/DMA/AuNPs remain in quenched state at normal tissues while only under acidic environment, the fluorescence can be restored. To investigate the three dimensional tumor mass, the tumors were collected and imaged by confocal microscope. The images were taken layer by layer in a 1 μm-step. As shown in Figure 5C, in the case when the mice are treated with PFBT/PLL-*g*-PEG/DMA/AuNPs, strong fluorescence in tumor tissue is observed. As control, the tissue from the mice treated with PFBT/PLL-*g*-PEG/SA/AuNPs shows weak fluorescence (Figure 5D). The three dimensional fluorescence image in various depth of tumor mass reveals that strong fluorescence can be detected up to 40 μm (Figure 5E), while only weak fluorescence from the control probe is observed (Figure 5F). These images indicate that the PFBT/PLL-*g*-PEG/DMA/AuNPs could be disassembled to yield strong fluorescence in tumor.

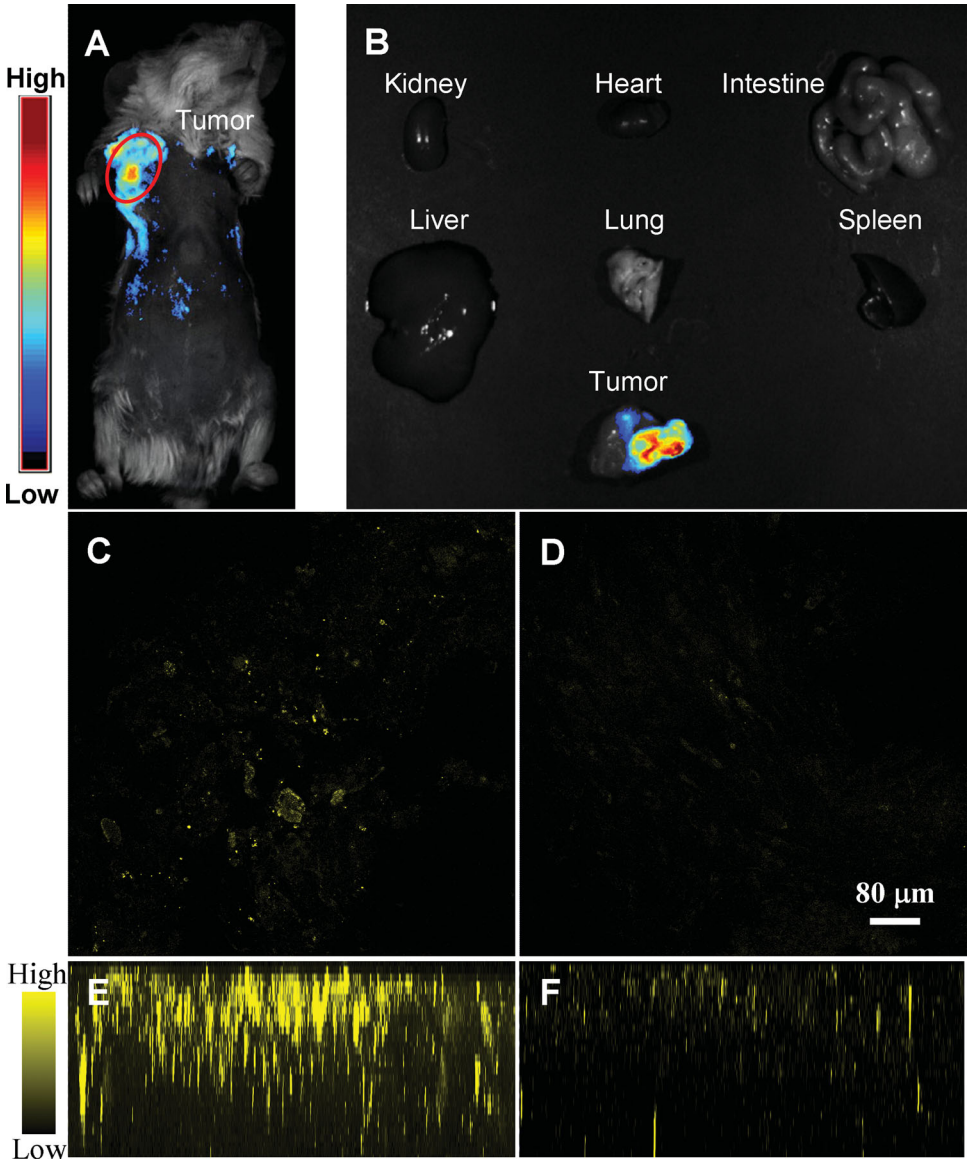

Figure 5. (A) In vivo non-invasive fluorescence images of tumor-bearing mice post intravenous injection of PFBT/PLL-*g*-PEG/DMA/AuNPs. The red circle indicates the tumor site. (B) Ex vivo fluorescence imaging of major normal organs and tumor tissue from mice treated with PFBT/PLL-*g*-PEG/DMA/AuNPs. The mice were sacrificed at 24 h post-injection. (C-F) Confocal images (5 μm deep) of the tumor tissue from mice administrated with PFBT/PLL-*g*-PEG/DMA/AuNPs (C) or PFBT/PLL-*g*-PEG/SA/AuNPs (D); The corresponding accumulative fluorescence images (40 μm) are shown in E and F, respectively.

The biocompatibility of a probe is crucial for biomedical applications.[37] The cytotoxicity of PFBT/PLL-*g*-PEG/DMA/AuNPs on U87-MG cells was assessed by MTT assays. The viabilities of U87-MG cells upon treatment with the hybrid at various concentrations were compared to the control. As shown in **Figure 6**A, no obvious toxicity is observed at the tested concentrations for 48 h, which demonstrates good biocompatibility of PFBT/PLL-*g*-PEG/DMA/AuNPs in vitro. Further in vivo toxicity studies were conducted by intravenously injecting PFBT/PLL-*g*-PEG/DMA/AuNPs to healthy tumor-free ICR mice using untreated healthy mice as the control group. After various administrations, the body weight changes of mice were monitored for 7 days. The body weight changes of mice in PFBT/PLL-*g*-PEG/DMA/AuNPs treated as well as untreated groups are shown in Figure 6B. As compared to the untreated control group, no noticeable body weight losses are observed. These results reveal that PFBT/PLL-*g*-PEG/DMA/AuNPs have no obvious in vivo toxicity to the mice, which hold great promises to serve as a safe and efficient fluorescent probe for in vivo applications.

3. Conclusion

In summary, we reported a novel platform for tumor imaging based on pH-responsive Au NP hybrid with high tumor specificity and sensitivity. The probe is non-fluorescent in physiological conditions but becomes highly emissive when exposed to tumoral acidic extracellular microenvironment. Moreover, their nanosized structures are suitable for efficient

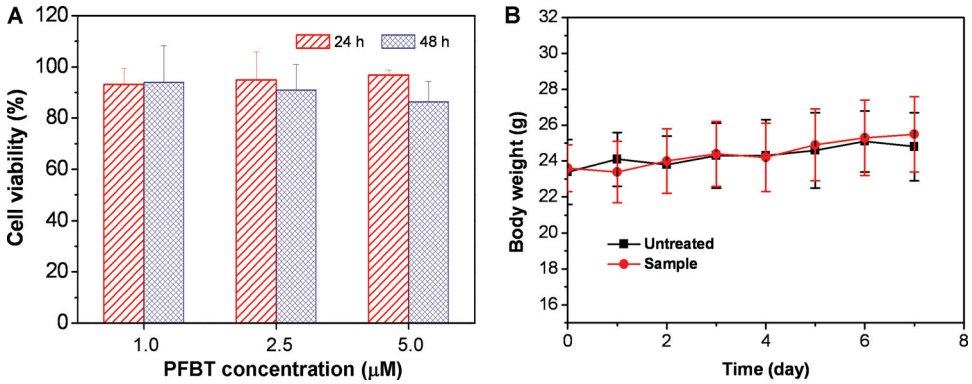

Figure 6. (A) Metabolic viability of U87-MG cells upon incubation with PFBT/PLL-*g*-PEG/DMA/AuNPs at different concentrations for 24 and 48 h; (B) Body weight changes of the mice with and without PFBT/PLL-*g*-PEG/DMA/AuNPs treatment (n = 4 mice per group) monitored for 7 days.

accumulation and fluorescence turn-on at tumor sites when intravenously administrated, which opens new opportunities for noninvasive in vivo imaging of tumors, and pH-responsive drug delivery in cancer therapy.

4. Experimental Section

Reagents and Chemicals: 2,3-Dimethylmaleic anhydride (DMA), O-methyl-O′-succinylpolyethylene glycol (MPEG-COOH, M_n = 2,000), poly-L-lysine hydrobromide (PLL·HBr, M_n = 5,000), hydrogen tetrachloroaurate(III) dehydrate ($HAuCl_4$), cysteamine, sodium borohydride, succinic anhydride (SA), anhydrous dimethyl sulfoxide, pyridine, triethylamine (TEA), 3-(4,5-dimethylthiazol-2-yl)-2,5-diphenyltetrazolium bromide (MTT) were purchased from Sigma-Aldrich and used as received. Deuterated dimethyl sulfoxide (d_6-DMSO) was purchased from Cambridge Isotope Laboratories, Inc. Conjugated polyelectrolyte poly[9,9-bis(6′-*N*,*N*,*N*-trimethylammonium)hexyl)fluorene-*alt*-4,7-(2,1,3-benzothiadiazole) dibromide] (PFBT, M_n = 6,000) was synthesized according to the reported methods.[26,38] 1× PBS contains NaCl (137 mM), KCl (2.7 mM), Na_2HPO_4 (10 mM), and KH_2PO_4 (1.8 mM). Dulbecco's modified essential medium (DMEM) was a commercial product of National University Medical Institutes (Singapore). Fetal bovine serum (FBS) and trypsin-EDTA solution were purchased from Gibco.

Instrumentation: UV-vis spectra were recorded on a Shimadzu UV-1700 spectrometer. PL spectra were measured on a Perkin-Elmer LS 55 spectrofluorometer. The particle size and size distribution were determined by laser light scattering (LLS) with a particle size analyzer (90 Plus, Brookhaven Instruments Co., USA) at a fixed angle of 90° at room temperature. The zeta potential of particles in aqueous solution was measured by Malvern Zetasizer Nano ZS90. Milli-Q water was supplied by Milli-Q Plus System (Millipore Corporation, Breford, USA). ^{1}H NMR spectra were measured on a Bruker ARX 400 NMR spectrometer. High-resolution transmission electron microscopy (HR-TEM) images were obtained from a JEOL JEM-2010 transmission electron microscope with an accelerating voltage of 200 kV.

Preparation of PLL-g-PEG/DMA and PLL-g-PEG/SA: PLL-*g*-PEG copolymer with PEG content of 8 mol% was prepared according to the previous method.[27] The residual amine groups of PLL-*g*-PEG were further reacted with anhydride. A typical procedure to amidize PLL using anhydrides is as follows: PLL-*g*-PEG (0.20 g, 0.52 mmol primary amine groups) and DMA (0.13 g, 1.04 mmol) were dissolved in anhydrous dimethyl sulfoxide (DMSO, 3 mL), then triethylamine (0.1 mL) and pyridine (0.1 mL) were added under N_2 atmosphere and the mixture was stirred at room temperature for 24 h. The resulting solution was precipitated into mixture of diethyl ether and acetone (v/v = 1:1). The precipitate was collected by filtration and dried under vacuum overnight to yield PLL-*g*-PEG/DMA (0.18 g, 55%). Succinic anhydride (SA) was grafted to PLL-*g*-PEG by a similar procedure to produce PLL-*g*-PEG/SA (0.12 g, 63%).

^{1}H NMR (400 MHz, d_6-DMSO): PLL-*g*-PEG/DMA: 4.21 (-NH-C$\underline{H}$(CH_2-)CO-), 3.53 (-C$\underline{H_2}$C$\underline{H_2}$-), 3.20 (-CH_2C$\underline{H_3}$), 3.08 (-$CH_2CH_2CH_2C\underline{H_2}$NH-), 1.73–1.81 (-COCH(C$\underline{H_3}$)CH(C$\underline{H_3}$)COOH), 1.59–1.67 (-C$\underline{H_2}CH_2CH_2CH_2$NH-), 1.51 (-$CH_2CH_2C\underline{H_2}CH_2$NH-), 1.28 (-$CH_2C\underline{H_2}CH_2CH_2$NH-).

PLL-*g*-PEG/SA: 4.21 (-NH-C$\underline{H}$(CH_2-)CO-), 3.53 (-C$\underline{H_2}$C$\underline{H_2}$-), 3.20 (-$CH_2C\underline{H_3}$), 3.08 (-$CH_2CH_2CH_2C\underline{H_2}$NH-), 2.32–2.38 (-COC$\underline{H_2}C\underline{H_2}$COOH), 1.59–1.67 (-C$\underline{H_2}CH_2CH_2CH_2$NH-), 1.51 (-$CH_2CH_2C\underline{H_2}CH_2$NH-), 1.28 (-$CH_2C\underline{H_2}CH_2CH_2$NH-).

Preparation of Positively-Charged AuNPs: Cysteamine-capped gold nanoparticles were prepared by reducing hydrogen tetrachloroaurate, $HAuCl_4$ in a liquid phase according to the literature.[34] Briefly, 100 μL of 213 mM cysteamine and 10 mL of 1.42 mM $HAuCl_4$ were mixed in a 50 mL glass vial. The mixture was stirring for 20 min at room temperature in the dark. Freshly prepared $NaBH_4$ (10 mM, 2.5 mL) was then quickly added into the above aqueous solution under vigorous stirring, and the mixture was further stirred for 60 min in the dark. The resulting wine-red solution was filtered through Millipore 0.45 μm filter and stored in the refrigerator (4 °C) before use. The as-prepared cysteamine-capped AuNPs were characterized with UV-vis absorption spectra, transmission electron microscopy (TEM) and dynamic light scattering (DLS), and zeta potential analysis.

Adsorption of PLL-g-PEG/DMA to the Positively-Charged AuNP: All glassware was washed with aqua regia before use. PLL-*g*-PEG/DMA was dissolved in water (5 mL, 1 mg/mL). Cysteamine-capped AuNP solution (1 mL) was added dropwise to the polymer solution using a glass pipet with vigorous stirring. The solution maintained a deep red color with very little color change. The solution was left stirring for 30 minutes. AuNPs were purified via centrifugation at 5,000 rpm for 10 minutes and redispersed in 10 mL of water. The process was repeated three times and the

obtained nanoparticles were characterized by UV-vis spectroscopy, TEM and DLS.

Assembly of PFBT/PLL-g-PEG/DMA/AuNPs: PFBT (0.4 mL, 20 μg/mL) was firstly dissolved in water/methanol mixture (v/v = 100/1) and carefully added to the above PLL-*g*-PEG/DMA-coated AuNP solution using a glass pipet with vigorous stirring. The solution was allowed to stir for 30 minutes. The free PFBT was removed by thorough ultrafiltration (Millipore, MWCO 100,000 Da). After repeating the process for three times, the obtained AuNPs were characterized by UV-vis spectroscopy, TEM and DLS.

General Procedure for Fluorimetric Assessment of Probe Activation: 50 μL of PFBT/PLL-*g*-PEG/DMA/AuNPs were diluted to 1 mL using phosphate buffered saline (PBS) of pH 6.5 or 7.4, respectively, and then incubated at 37 °C. At designated time intervals, the change of zeta potential and fluorescence intensity was measured. The solution was excited at 440 nm, and the emission was collected from 500 to 800 nm.

Cell Culture: U87-MG glioma cancer cells were provided by American Type Culture Collection (ATCC). The cells were cultured in DMEM (Invitrogen, Carlsbad, CA) containing 10% heat-inactivated FBS (Invitrogen), 100 U/mL penicillin, and 100 μg/mL streptomycin (Thermo Scientific) and maintained in a humidified incubator at 37 °C with 5% CO_2. Before experiment, the cells were precultured until confluence was reached.

Confocal Imaging: U87-MG cells were cultured in the chambers (LAB-TEK, Chambered Coverglass System) at 37 °C. After 80% confluence, the culture medium was replaced with 400 μL of fresh medium containing the AuNP hybrid (1.0 μM PFBT) at pH 7.4 or 6.5. After incubation at 37 °C for 1 h, the cells were washed twice with ice-cold PBS and fixed with fresh 4% paraformaldehyde for 10 min at room temperature and permeabilized with 0.1% Triton X-100 in 1 × PBS for 5 min. The cells were stained with propidium iodide (Invitrogen, Carlsbad, CA) for the cell nucleus following the standard protocol of the manufacturer. The cells were then imaged immediately by confocal laser scanning microscope (CLSM, Zeiss LSM 410, Jena, Germany) with imaging software (Fluoview FV500). The images were analyzed by Image J1.43 × program (developed by NIH, http://rsbweb.nih.gov/ij/).

Flow Cytometry Study: Five groups of U87-MG cancer cells were precultured in culture flask to achieve desired confluence, respectively. One group was used as the control without treatment. For the rest groups, the medium was replaced with 400 μL of fresh medium containing the Au NP hybrid (1.0 μM PFBT) at pH 7.4 or 6.5, which were followed by incubation for 1 h at 37 °C, respectively. The control and sample groups were treated with trypsin and washed with DMEM medium through centrifugation. The cell density was measured using a hemocytometer. Approximately 5×10^5 of U87-MG cancer cells were dispersed in 2 mL of DMEM medium for both control and the sample groups. Flow cytometry measurements were conducted using Cyan-LX (DakoCytomation). The mean fluorescence was determined by counting 10,000 events (Ex 488 nm).

Biodistribution of the Nanoparticles: When the C6 glioma tumor volume reached a mean size of about 150 mm^3, the mice were intravenously injected with 100 μL of samples (1.0 mg PFBT/kg). The mice were then anesthetized and placed on an animal plate heated to 37 °C. The biodistribution of the samples in C6 tumor-bearing mice was imaged using a Maestro EX in vivo fluorescence imaging system (CRi, Inc.). The light with a central wavelength at 457 nm was selected as the excitation source. In vivo spectral imaging from 500 nm to 900 nm (10 nm step) was carried out with an exposure time of 150 ms for each image frame. The auto-fluorescence was removed using spectral unmixing software. Scans were carried out at 24 h post-injection, respectively. In addition, at 24 h post-injection, the tumor-bearing mice intravenously injected with the samples were sacrificed and the tissues including kidney, heart, intestine, liver, lung, spleen and tumor were isolated and imaged using the Maestro system for ex vivo fluorescence imaging.

Ex Vivo Tumor Imaging: The animal experiments for ex vivo study were performed in compliance with guidelines set by the Institutional Animal Care and Use Committee (IACUC), Singapore General Hospital. C6 glioma cell suspension containing 1×10^6 cells (0.1 mL) was injected subcutaneously to the left flank of BALB/c nude mice. When the tumor volume reached a mean size of about 200 mm^3, the mice were intravenously injected with 100 μL of AuNP hybrid (1.0 mg PFBT/kg). At 24 h post-injection, the tumor tissues were excised, fixed in 4% paraformaldehyde and then imaged by Leica TCS SP 5X and multiphoton microscope. Fluorescence images of consecutive layers with 1 μm per layer were recorded to generate 3D reconstruction to investigate the intensity and penetration depth of fluorescence from PFBT under excitation upon 488 nm.

Cytotoxicity of PFBT/PLL-g-PEG/DMA/AuNPs: 3-(4,5-Dimethythiazol-2-yl)-2,5-diphenyltetrazolium bromide (MTT) assays were used to assess the metabolic activity of U87-MG cancer cells to study the cytotoxicity of our probes. U87-MG cells were seeded in 96-well plates (Costar, IL, USA) at an intensity of 4×10^4 cells mL^{-1}. After 24 h incubation, the medium was replaced by the probe suspension at different concentrations. After incubation at 37 °C for 2 h, the medium was replaced with fresh DMEM and incubated at 37 °C. After the designated time intervals, the wells were washed twice with 1 × PBS buffer, and 100 μL of freshly prepared MTT (0.5 mg mL^{-1}) solution in culture medium was added into each well. The MTT medium solution was carefully removed after 3 h incubation in the incubator at 37 °C. DMSO (100 μL) was then added into each well and the plate was gently shaken to dissolve all the precipitates formed. The absorbance of MTT at 570 nm was monitored by the microplate reader (GeniosTecan). Cell viability was expressed by the ratio of absorbance of the cells incubated with probe suspension to that of the cells incubated with culture medium only.

Acknowledgements

We thank the Singapore National Research Foundation (R-279–000–390–281), the SMART (R279–000–378–592), and the Institute of Materials Research and Engineering of Singapore (IMRE/12–8P1103) for financial support.

[1] D. E. Lee, H. Koo, I. C. Sun, J. H. Ryu, K. Kim, I. C. Kwon, *Chem. Soc. Rev.* **2012**, *41*, 2656.
[2] K. Y. Choi, G. Liu, S. Lee, X. Y. Chen, *Nanoscale* **2012**, *4*, 330.

[3] X. Lin, J. Xie, L. Zhu, S. Lee, G. Niu, Y. Ma, K. Kim, X. Y. Chen, *Angew. Chem. Int. Ed.* **2011**, *50*, 1569.
[4] S. Lee, K. Park, K. Kim, K. Choi, I. C. Kwon, *Chem. Commun.* **2008**, 4250.
[5] S. Lee, J. H. Ryu, K. Park, A. Lee, S. Y. Lee, I. C. Youn, C. H. Ahn, S. M. Yoon, S. J. Myung, D. H. Moon, X. Chen, K. Choi, I. C. Kwon, K. Kim, *Nano Lett.* **2009**, *9*, 4412.
[6] T. Jiang, E. S. Olson, Q. T. Nguyen, M. Roy, P. A. Jennings, R. Y. Tsien, *Proc. Natl. Acad. Sci. USA* **2004**, *101*, 17867.
[7] P. RiveraGil, M. Nazarenus, S. Ashraf, W. J. Parak, *Small* **2012**, *8*, 943.
[8] H. Lee, W. Akers, K. Bhushan, S. Bloch, G. Sudlow, R. Tang, S. Achilefu, *Bioconjug. Chem.* **2011**, *22*, 777.
[9] J. Y. Ko, S. Park, H. Lee, H. Koo, M. S. Kim, K. Choi, I. C. Kwon, S. Y. Jeong, K. Kim, D. S. Lee, *Small* **2010**, *6*, 2539.
[10] T. Yoshitomi, R. Suzuki, T. Mamiya, H. Matsui, A. Hirayama, Y. Nagasaki, *Bioconjug. Chem.* **2009**, *20*, 1792.
[11] Y. Urano, D. Asanuma, Y. Hama, Y. Koyama, T. Barrett, M. Kamiya, T. Nagano, T. Watanabe, A. Hasegawa, P. L. Choyke, H. Kobayashi, *Nat. Med.* **2009**, *15*, 104.
[12] R. A. Cardone, V. Casavola, S. J. Reshkin, *Nat. Rev. Cancer* **2005**, *5*, 786.
[13] X. M. Zhang, Y. X. Lin, R. J. Gillies, *J. Nucl. Med.* **2010**, *51*, 1167.
[14] M. Oishi, S. Sumitani, Y. Nagasaki, *Bioconjug. Chem.* **2007**, *18*, 1379.
[15] R. van Sluis, Z. M. Bhujwalla, N. Raghunand, P. Ballesteros, J. Alvarez, S. Cerdan, J. P. Galons, R. J. Gillies, *Magn. Reson. Med.* **1999**, *41*, 743.
[16] R. J. Gillies, Z. Liu, Z. Bhujwalla, *Am. J. Physiol.* **1994**, *267*, C195.
[17] D. A. Rottenberg, J. Z. Ginos, K. G. Kearfott, L. Junck, V. Dhawan, J. O. Jarden, *Ann. Neurol.* **1985**, *17*, 70.
[18] D. Ding, G. Wang, J. Liu, K. Li, K.-Y. Pu, Y. Hu, J. C. Y. Ng, B. Z. Tang, B. Liu, *Small* **2012**, *8*, 3523.
[19] C. L. Zhu, L. B. Liu, Q. Yang, F. T. Lv, S. Wang, *Chem. Rev.* **2012**, *112*, 4687.
[20] X. L. Feng, L. B. Liu, S. Wang, D. B. Zhu, *Chem. Soc. Rev.* **2010**, *39*, 2411.
[21] K. Y. Pu, B. Liu, *Adv. Funct. Mater.* **2011**, *21*, 3408.
[22] J. Liang, K. Li, B. Liu, *Chem. Sci.* **2013**, *4*, 1377.
[23] Q. Zhou, T. M. Swager, *J. Am. Chem. Soc.* **1995**, *117*, 12593.
[24] K. Y. Pu, K. Li, X. H. Zhang, B. Liu, *Adv. Mater.* **2010**, *22*, 4186.
[25] Y. S. Wang, B. Liu, A. Mikhailovsky, G. C. Bazan, *Adv. Mater.* **2010**, *22*, 656.
[26] K. Y. Pu, B. Liu, *Adv. Funct. Mater.* **2009**, *19*, 277.
[27] M. Lee, S. O. Han, K. S. Ko, J. J. Koh, J. S. Park, J. W. Yoon, S. W. Kim, *Mol. Ther.* **2001**, *4*, 339.
[28] Z. X. Zhou, Y. Q. Shen, J. B. Tang, M. H. Fan, E. A. Van Kirk, W. J. Murdoch, M. Radosz, *Adv. Func. Mater.* **2009**, *19*, 3580.
[29] J. Z. Du, X. J. Du, C. Q. Mao, J. Wang, *J. Am. Chem. Soc.* **2011**, *133*, 17560.
[30] A. J. Gormley, N. Larson, S. Sadekar, R. Robinson, A. Ray, H. Ghandehari, *Nano Today* **2012**, *7*, 158.
[31] M. J. Sailor, J.-H. Park, *Adv. Mater.* **2012**, *24*, 3779–3802.
[32] C. Rosman, S. Pierrat, A. Henkel, M. Tarantola, D. Schneider, E. Sunnick, A. Janshoff, C. Sönnichsen, *Small* **2012**, *8*, 3683.
[33] S. T. Kim, A. Chompoosor, Y.-C. Yeh, S. S. Agasti, D. J. Solfiell, V. M. Rotello, *Small* **2012**, *8*, 3253.
[34] Y. Jv, B. X. Li, R. Cao, *Chem. Commun.* **2010**, *46*, 8017.
[35] C. H. Fan, S. Wang, J. W. Hong, G. C. Bazan, K. W. Plaxco, A. J. Heeger, *Proc. Natl. Acad. Sci. U.S.A* **2003**, *100*, 6297.
[36] J. Fang, H. Nakamura, H. Maeda, *Adv. Drug. Delivery Rev.* **2011**, *63*, 136.
[37] D. S. Kohane, R. Langer, *Chem. Sci.* **2010**, *1*, 441.
[38] B. Liu, G. C. Bazan, *Nat. Protoc.* **2006**, *1*, 1698.

Received: August 24, 2013
Revised: November 15, 2013
Published online: March 10, 2014

